


Communication

# Simultaneous Removal of Residual Sulfate and Heavy Metals from Spent Electrolyte of Lead-Acid Battery after Precipitation and Carbonation

Shuai Gu <sup>1</sup> , Bitian Fu <sup>2</sup> and Ji Whan Ahn <sup>1,\*</sup>

<sup>1</sup> Center for Carbon Mineralization, Mineral Resources Division, Korea Institute of Geoscience and Mineral Resources, Daejeon 34132, Korea; gushuai@kigam.re.kr

<sup>2</sup> Shanghai Environment Sanitation Engineering Design and Research Institute Co. Ltd., Shanghai 200232, China; bitianfu@hotmail.com

\* Correspondence: ahnjw@kigam.re.kr

Received: 2 January 2020; Accepted: 4 February 2020; Published: 10 February 2020



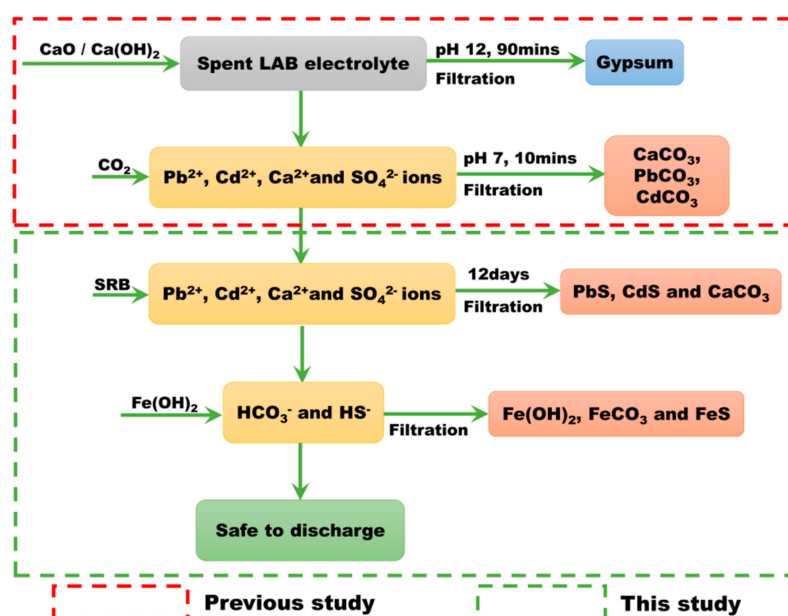
**Abstract:** Spent electrolyte from lead-acid battery contains high concentrations of sulfate acid and heavy metals; therefore without proper handling, they might cause severe environmental pollution. A relatively high concentration of sulfate ions (approximately 3000 mg/L) and heavy metals still exists in the effluent even after precipitation with slaked lime and carbonation process, which need to be further processed to lower both the concentrations of sulfate and heavy metals for direct discharge. A process that involves the reduction of sulfate to sulfide with sulfate-reducing bacteria and precipitation of the excessive sulfide with  $\text{Fe}(\text{OH})_2$  was adopted to dispose of the effluent after precipitation and carbonation for direct discharge. Thermodynamic calculations were adopted to narrow down the optimum experimental range and understand the precipitation mechanism. In the whole process, no new impurities nor ions were introduced and 99.2% of sulfate, 99.9% of sulfide, 99.1% of Ca and more than 94.6% of Pb and 99.8% of Cd were removed and the obtained effluent was safe to discharge.

**Keywords:** sulfate removal; spent lead-acid battery; heavy metals; sulfate-reducing bacteria

## 1. Introduction

Lead-acid batteries (LABs), composed of grid (Pb), lead paste ( $\text{PbO}$ ,  $\text{PbO}_2$ ,  $\text{PbSO}_4$ ), electrolytes (36–39%  $\text{H}_2\text{SO}_4$ ), and shells, are generally utilized as rechargeable power storage devices, e.g., stand-alone power systems [1–3], motor vehicles [4,5], and backup power supplies [6–8]. As the main component of LAB, the majority of lead (approximately 85%) is consumed in the production process [9], which encourages the recycling of spent LABs. The recycling of lead grid and plastics have already been commercialized [10–12], while the recycling of lead paste and electrolyte are still under intense investigation [13–17]. Spent electrolyte from LABs contains high concentrations of sulfate acid and a certain amount of heavy metals, which are highly corrosive and poisonous and could cause serious environmental crises without proper disposal methods. [18] LABs, as one of the major sources of lead exposure worldwide, can cause many adverse clinical outcomes in children and adults, [19] especially, for fetuses and gravidas since lead exposure can occur at each stage of pregnancy [20,21]. The adverse effect caused by lead exposure continues during the life course [22] and affects several key organ systems, e.g., the cardiovascular [23], renal [24,25], and hepatic [26,27] systems. Depending on the concentration of sulfate ions, wastewater is disposed of by precipitation with lime or slaked lime [16,28], crystallization [29] for solutions with high sulfate concentration and exchange resin [30], and sulfate-reducing bacteria (SRB) [31–35] for solutions with low sulfate concentration. Compared

with other techniques, SRB methods have the advantages of high removal ratio, low capital, and operation cost and are capable of large scale operation at low sulfate concentrations and medium pH range. The mechanism and kinetics of reducing sulfate with different SRB under different pH, heavy metal concentrations, and carbon sources have already been investigated in detail [31–41]. However, there is very little research reported on the removal of the reduced product, i.e., sulfide, from the resulting solution to meet the standards for direct discharge. In our previous study, as shown in Scheme 1 (refer to box with red dashed line), slaked lime and CO<sub>2</sub> was utilized to remove the majority of sulfate and heavy metals (Pb and Cd) from spent LAB electrolyte with the theoretical removal ratio of sulfate around 99% [15] and experimental removal ratio of sulfate around 97% [16] by precipitation and carbonation. The theoretical removal ratio was mainly determined by the solubility products of gypsum. Even after precipitation and carbonation process, a certain amount of sulfate (around 3000 mg/L) and heavy metals still exist in the effluent, which is too high for direct discharge.



**Scheme 1.** Illustration of the disposal approach to recycle LAB electrolyte.

In this study, we focused on the removal of sulfide obtained from sulfate by SRB and other hazardous elements (Pb and Cd) to meet the standard for direct discharge. Hereby, a two-step process, as shown in Scheme 1 (refer to box with green dashed line), was proposed and utilized to remove sulfate, sulfide that originated from sulfate, heavy metals (Pb and Cd), and Ca<sup>2+</sup> from the effluent of spent LAB electrolyte. In the first step, SRB was utilized to remove sulfate from the effluent by precipitation and carbonation process, and the resulting sulfide was then utilized to precipitate the heavy metals in the effluent. In the next step, the sediment was filtered and Fe(OH)<sub>2</sub> was added to remove the excessive sulfide as FeS. Both thermodynamic modeling and experiments were adopted to interpret and optimize the recycling process. Thermodynamic calculations were utilized to understand the precipitation mechanism and narrow down the optimum recycling conditions.

## 2. Materials and Methods

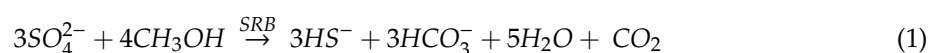
### 2.1. Materials

The spent LAB electrolyte effluent was obtained from the precipitation and carbonation process as described in our previous study [16]. The SRB utilized in the study was a mixed culture obtained from the local wastewater plant and cultured with Postgate C (0.5 g/L K<sub>2</sub>HPO<sub>4</sub>, 1.0 g/L NH<sub>4</sub>Cl, 4.5 g/L Na<sub>2</sub>SO<sub>4</sub>, 0.06 g/L CaCl<sub>2</sub>•6H<sub>2</sub>O, 0.06 g/L MgSO<sub>4</sub>•7H<sub>2</sub>O, 6.0 g/L sodium lactate, 1.0 g/L yeast, 0.004 g/L

$\text{FeSO}_4 \bullet 7\text{H}_2\text{O}$ , 0.3 g/L sodium citrate  $\bullet 2\text{H}_2\text{O}$ , and 25 g/L NaCl) [36]. Lactate was reported as the optimum carbon source for SRB [37], however, in this study, to avoid the release of acetate from the partial degradation process [38,39], methanol was utilized [40]. Before utilization, SRB was pre-grown and cultivated in the Postgate C medium with an incubating time of one month. After this, the enriched community was inoculated to the effluent to start the sulfate reduction process. The bacteria proved to be Gram-negative species. The initial methanol concentration, redox potential, and temperature of the effluent were kept at 4 g/L, 0.1V, and 30 °C, respectively. Table 1 shows the initial concentration of effluent obtained after the precipitation and carbonation process, with the main components being  $\text{Ca}^{2+}$  (400.1 mg/L) and  $\text{SO}_4^{2-}$  (3013.5 mg/L) with pH 7.01. Two heavy metals, i.e., Pb and Cd, were detected with a concentration of 0.924 and 2.10 mg/L, respectively.

## 2.2. Methods

The reduction of sulfate to sulfide was conducted according to Equation (1) in the batch experiments with immobilized SRB in a 1 L glass vessel [41]. The concentration of  $\text{SO}_4^{2-}$ ,  $\text{HS}^-$ , and  $\text{HCO}_3^-$  were measured with spectrophotometric method (HS-3300 Water analyzer & spectrophotometer, HUMAS) [42], 4500- $\text{S}^{2-}$  method [43], and Raman spectroscopy (DXR Smart Raman spectrometer, Thermo Fisher Scientific Inc.) [44], respectively (detailed information can be found in Supporting Information). The concentration of metal ions ( $\text{Ca}^{2+}$ ,  $\text{Pb}^{2+}$ ,  $\text{Cd}^{2+}$ , and  $\text{Fe}^{2+}$ ) were measured with Inductively coupled plasma - optical emission spectrometry (ICP-OES) (PerkinElmer® Optima 5300 DV). pH was monitored by a Thermo Scientific pH meter equipped with a highly sensitive ROSS electrode. The parameters of the reduction process were monitored every two days.



After the reduction of sulfate, the precipitate was filtered, the effluent then further precipitated with fresh  $\text{Fe}(\text{OH})_2$  (6.29 g/L) to remove sulfide for 24h at 200 rpm stirring, after which the obtained precipitate was also filtered. Both precipitates were dried at 80 °C for 48h and analyzed with X-ray powder diffraction (XRD). The precipitation and removal process were simulated by thermodynamic calculations with Matlab® R2010a. All thermodynamic parameters (Table S1, Supporting Information) and ionic strength were taken into consideration according to our previous study [15].

## 3. Results and Discussion

### 3.1. Sulfate Reduction and Heavy Metal Removal

#### 3.1.1. Sulfate Reduction with SRB

The treatment starts with the reduction of sulfate to sulfide by SRB, as shown in Figure 1. The batch experiments show the reduction kinetics of sulfate in a sterilized anaerobic medium. A decrease in sulfate concentration at around 99% was observed within 12 days in the immobilized batch reactor. The pH increased sharply in the first 4 days from 7.01 to 8.34 and then slowly increased to 8.81 on day 12. The mean sulfate reduction rate in the first 12 days was 10.36 mg/h. The concentration of ions in the effluent after 12 days of reduction is shown in Table 1, and as seen, the majority of  $\text{Ca}^{2+}$ ,  $\text{SO}_4^{2-}$ ,  $\text{Pb}^{2+}$ , and  $\text{Cd}^{2+}$  were removed in the sulfate reduction process.

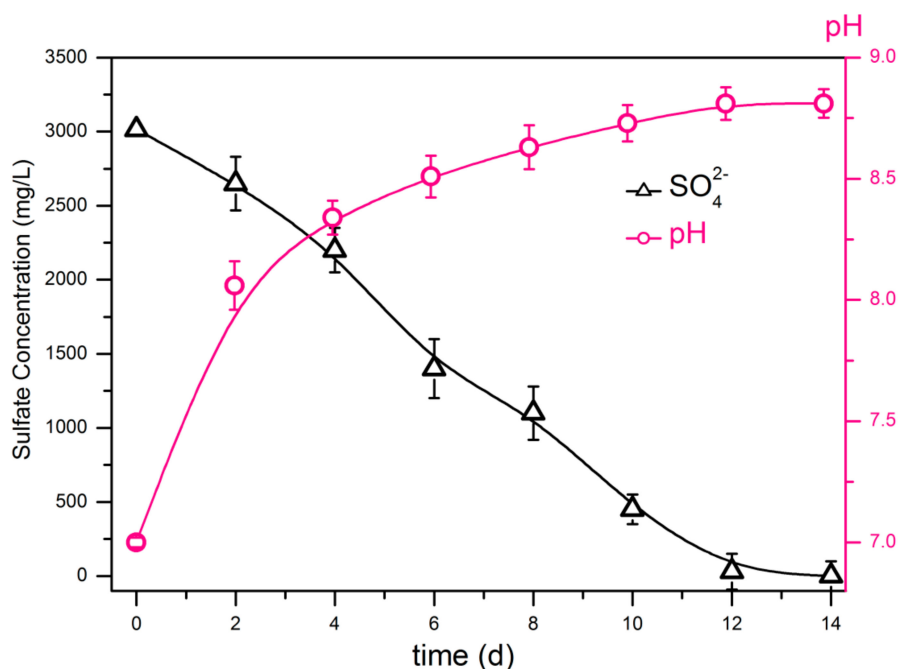


**Figure 1.** Sulfate concentration and pH value in the batch reactor with pre-grown mixed SRB.

### 3.1.2. $\text{Pd}^{2+}$ , $\text{Cd}^{2+}$ and $\text{Ca}^{2+}$ Removal

According to Equation (1) in the sulfate reduction process, sulfate was reduced to sulfide with the electrons from methanol, with the assistance of SRB, resulting in the existence of both sulfide and bicarbonate. The concentration of sulfide and bicarbonate increased with the reaction time, until the ion products ( $Q_{sp}$ ) of  $\text{PbS}$ ,  $\text{CdS}$ , and  $\text{CaCO}_3$  in the solution are larger than their solubility products ( $K_{sp}$ ), resulting in precipitation of excess ions from the solution as solids. To predict the extent of the reaction between sulfide and bicarbonate with  $\text{Pd}^{2+}$ ,  $\text{Cd}^{2+}$ , and  $\text{Ca}^{2+}$ , thermodynamic calculations were carried out on the assumption that 99% sulfate was reduced to sulfide and the same amount of bicarbonate was also produced according to the stoichiometric number. The detailed results are shown in Figure 2. Figure 2a shows the concentrations of all ions in the effluent *vs.* pH; as seen, several precipitates exist in the effluent, i.e.,  $\text{CaCO}_3$ ,  $\text{PbS}$ , and  $\text{CdS}$ . The parameters used in the calculation process is shown in Table 1. Equations (S1)–(S27) (Table S1, Supporting Information) were utilized to calculate the equilibrium after the sulfate reduction process. Four kinds of cadmium complex ( $\text{CdHS}^+$ :  $\log K = 8.24$ ,  $\text{Cd}(\text{HS})_2$ :  $\log K = 15.46$ ,  $\text{Cd}(\text{HS})_3^-$ :  $\log K = 17.36$  and  $\text{Cd}(\text{HS})_4^{2-}$ :  $\log K = 19.32$ ) [45] and three kinds of lead complex ( $\text{PbHCO}_3^-$ :  $\log K = 13.35$ ,  $\text{PbCO}_3$ :  $\log K = 6.6$ ,  $\text{Pb}(\text{CO}_3)_2^{2-}$ :  $\log K = 10.1$ ) were taken into consideration, while three kinds of both cadmium precipitates ( $\text{Cd}(\text{OH})_2$ :  $\log K = -13.65$ ,  $\text{CdCO}_3$ :  $\log K = 12.1$  and  $\text{CdS}$ :  $\log K = 14.13$ ) and lead precipitates ( $\text{Pb}(\text{OH})_2$ :  $\log K = -13.6$ ,  $\text{PbCO}_3$ :  $\log K = 13.2$ , and  $\text{PbS}$ :  $\log K = 14.86$ ) were selected as possible precipitates. As can be seen,  $\text{CdS}$  and  $\text{PbS}$  precipitate are the main species for cadmium and lead ions in the whole pH range [46], while  $\text{CaCO}_3$  is the main species for calcium when  $\text{pH} > 6.2$ . A typical distribution of sulfide ions was observed in Figure 2b with  $\text{H}_2\text{S}$ ,  $\text{HS}^-$ , and  $\text{S}^{2-}$  being the main species in low ( $\text{pH} < 7$ ), medium ( $7 < \text{pH} < 12$ ), and high ( $12 < \text{pH} < 14$ ) pH range, respectively. Due to relatively low concentration, no  $\text{H}_2\text{S}$  gas was observed in the calculation even in the high acid region. The fraction of bicarbonate shown in Figure 2c suggested that both soluble carbon dioxide ( $\text{CO}_2$ ), carbonic acid ( $\text{H}_2\text{CO}_3$ ), bicarbonate ( $\text{HCO}_3^-$ ), and carbonate ( $\text{CO}_3^{2-}$ ) ions exist in different pH regions. Due to the existence of calcium ions and the fact that the  $Q_{sp}(\text{CaCO}_3) > K_{sp}(\text{CaCO}_3)$ , calcium carbonate precipitate ( $\text{CaCO}_3$ ) started to appear when  $\text{pH} > 6.2$ . A similar distribution of carbonate ions can also be observed as sulfide ions with  $\text{CO}_2$  and  $\text{H}_2\text{CO}_3$  being the main species when  $\text{pH} < 6$ ,  $\text{HCO}_3^-$  dominates when  $6 < \text{pH} < 10$ , and  $\text{CO}_3^{2-}$  dominates when  $10 < \text{pH} < 14$ . For calcium ions, five species ( $\text{CaCO}_3$ :  $\log K = 3.339$ ,  $\text{CaHCO}_3^-$ :  $\log K = 11.44$ ,  $\text{CaOH}^+$ :

$\log K = -12.83$ ,  $\text{CaCO}_3(\text{s})$ :  $\log K = 8.3$ ,  $\text{Ca}(\text{OH})_2(\text{s})$ :  $\log K = -22.62$ ) were considered in the whole pH range, as shown in Figure 2d, and three species were observed, i.e.,  $\text{Ca}^{2+}$  ( $\text{pH} < 9$ ),  $\text{CaHCO}_3^+$  ( $5 < \text{pH} < 8$ ), and  $\text{CaCO}_3(\text{s})$  ( $6.2 < \text{pH}$ ). For lead (Figure 2e) and cadmium (Figure 2f), the circumstances were much simpler, with the precipitates being the main species in almost the whole pH range ( $1 < \text{pH} < 14$ ), which suggested that the precipitates ( $\text{PbS}$  and  $\text{CdS}$ ) are extremely stable in the effluent. According to the final pH measured, after sulfate reduction, the main species for all related ions were  $\text{HS}^-$  for sulfide ions,  $\text{HCO}_3^-$  for bicarbonate ions,  $\text{CaCO}_3(\text{s})$  for calcium ions,  $\text{PbS}$  for lead ions, and  $\text{CdS}$  for cadmium ions.

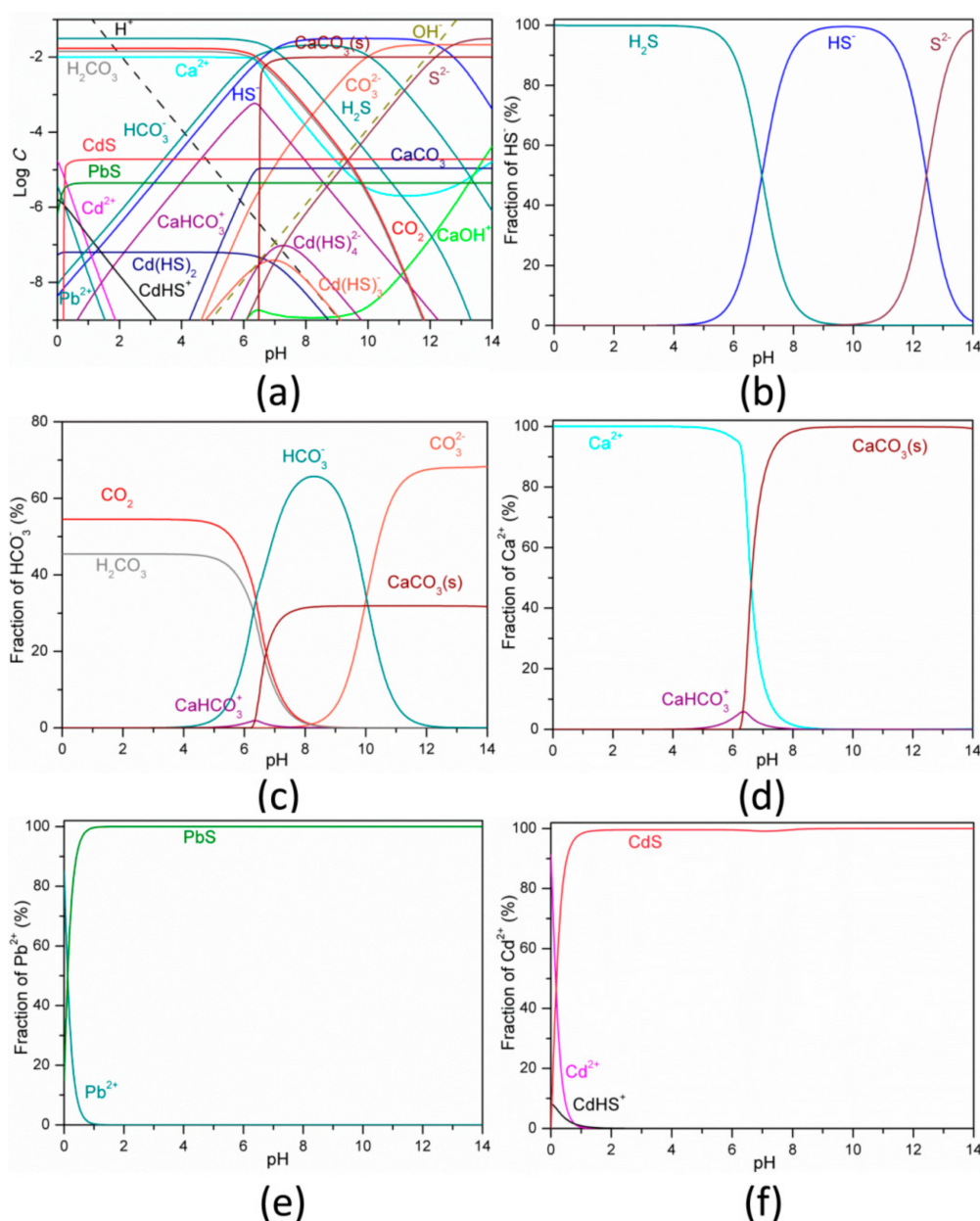


**Figure 2.** Calculated species distributions of the effluent after the sulfate reduction process: (a) Distributions of all elements in the effluent at equilibrium *vs.* pH; (b) Fraction of sulfide ions in the effluent *vs.* pH; (c) Fraction of bicarbonate ions in the effluent *vs.* pH; (d) Fraction of calcium ions in the effluent *vs.* pH; (e) Fraction of lead ions in the effluent *vs.* pH; (f) Fraction of cadmium ions in the effluent *vs.* pH.

After the sulfate reduction process, a certain amount of black sediment was filtered and analyzed with XRD (Figure 3). As can be seen from the graph, three different phases were observed, i.e., calcite ( $\text{CaCO}_3$ ), galena ( $\text{PbS}$ ), and hawleyite ( $\text{CdS}$ ). The main composition was calcite (96%), while  $\text{PbS}$  and  $\text{CdS}$  both count for approximately 2% of the sediment. This result was in good accordance with the thermodynamic simulation results. After the sulfate reduction process, 99.1%  $\text{SO}_4^{2-}$ , >99.8%  $\text{Cd}^{2+}$ , >94.6%  $\text{Pb}^{2+}$ , and 99.1%  $\text{Ca}^{2+}$  were removed according to the results shown in Table 1. Considering the detection limit of ICP-OES for Pb (0.05 mg/L) and Cd (0.005 mg/L), the removal ratios of Pb and Cd were calculated based on the lowest detection limit. In Table 1, the removal ratios of Pb and Cd were calculated to be larger than 94.6% and 99.8%, respectively, since the concentrations of Pb and Cd after precipitation were out of the detection limit (ODL).

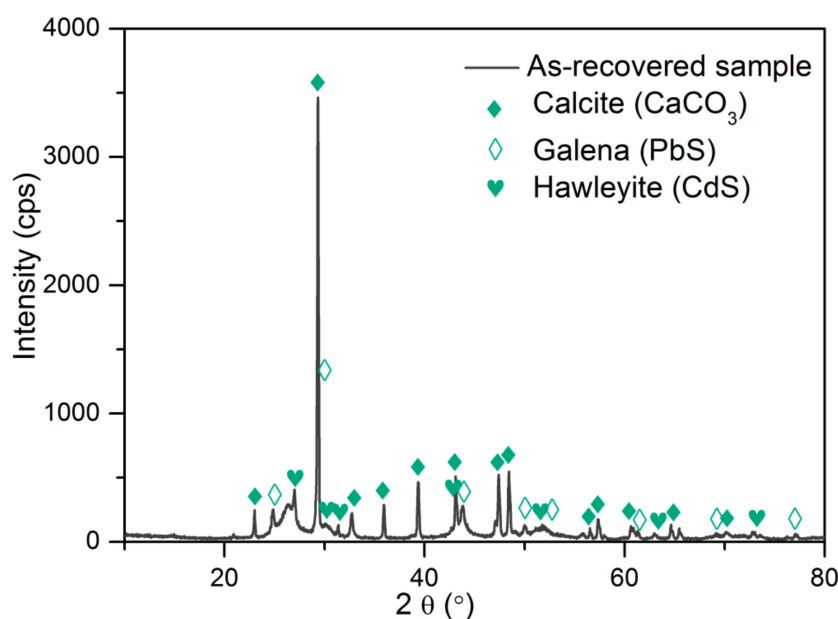
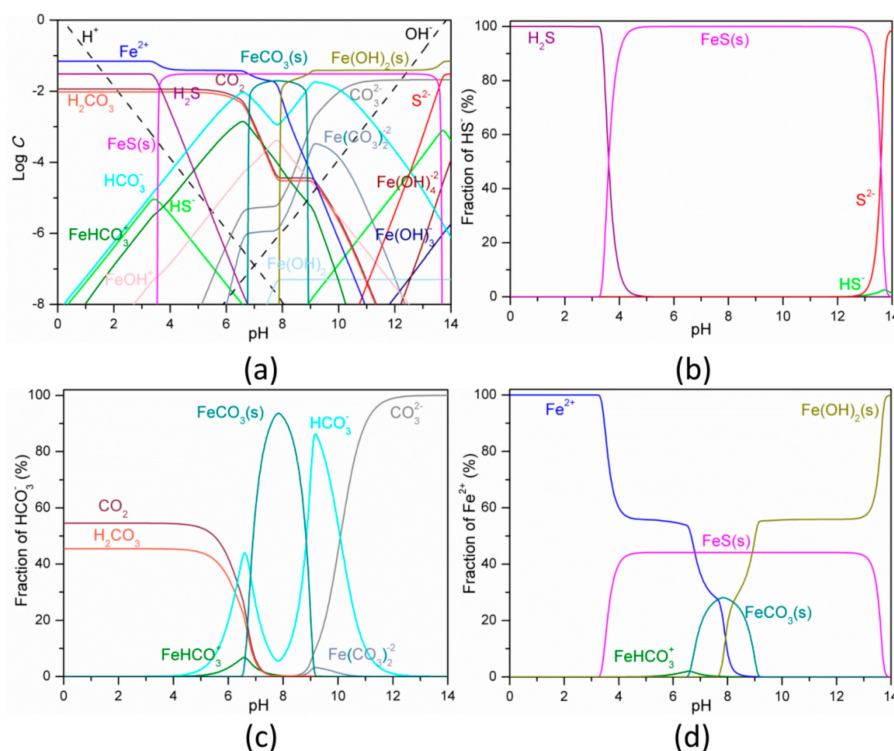


Figure 3. XRD pattern of the sediment obtained from the sulfate reduction process.

### 3.2. Sulfide Precipitation

After the sulfate reduction process, both heavy metals (Pb and Cd) and calcium ions were removed from the solution. However, a large amount of sulfide and bicarbonate ions were produced and existed in the effluent. Due to the rotten egg smell and toxicity of sulfide ions, a precipitation step was added to remove the hazardous sulfide ions. To avoid introducing new impurities into the effluent,  $\text{Fe}(\text{OH})_2$  was selected as the precipitation agent for removing sulfide. In the precipitation process, excessive  $\text{Fe}(\text{OH})_2$  was added, and the reaction mechanism was simulated by thermodynamic calculations as shown in Figure 4.





**Figure 4.** Calculated species distributions of the effluent after the sulfide precipitation: (a) Distribution vs. pH; (b) Fraction of sulfide ion vs. pH (c) Fraction of bicarbonate ion vs. pH; (d) Fraction of iron ions vs. pH.

Figure 4a shows the simulated species distributions in the sulfide precipitation process. Equations (S1), (S12)–(S18), and (S28)–(S35) (Table S1, Supporting Information) were utilized to simulate the equilibrium distributions. Eight species of iron, including four complexes ( $Fe(CO_3)_2^{2-}$ :  $\log K = 20.53$ ,  $FeHCO_3^+$ :  $\log K = 24.93$ ,  $Fe(OH)_3^-$ :  $\log K = -19.9$  and  $Fe(OH)_4^{2-}$ :  $\log K = -32.85$ ) and three precipitates ( $Fe(OH)_2(s)$ :  $\log K = -7.3$ ,  $FeCO_3(s)$ :  $\log K = 21.22$  and  $FeS(s)$ :  $\log K = 16.95$ ) were taken into consideration in the calculation process. Three precipitates were observed, i.e.,  $Fe(OH)_2$ ,  $FeCO_3$ ,  $FeS$ , in different pH ranges. The simulation was calculated according to the results shown in Table 1. As can be seen from Figure 4b, three sulfide containing species were observed with  $H_2S$  being the main species when  $pH < 4$ ,  $FeS$  dominates in  $4 < pH < 13$  and  $S^{2-}$  exists in  $12 < pH < 14$ . Where the pH ranged from 5 to 12.5, all sulfide was observed in the form of  $FeS$ . As for bicarbonate ions, similar distributions were observed (Figure 2c) while, due to the adding of iron, a certain amount of  $FeCO_3$  may also be observed in the pH range of 6.5 to 9.2. Two complexes  $FeHCO_3^+$  and  $Fe(CO_3)_2^{2-}$  were also observed in pH 5 to 8 and 8.5 to 10, respectively. As can be seen (Figure 4d), five out of the eight calculated species were observed, which involved all three precipitates ( $Fe(OH)_2$ ,  $FeCO_3$ , and  $FeS$ ) and one complex ( $FeHCO_3^+$ ).  $FeS$  precipitate can be observed in a relatively wide pH range from 3.2 to 14, while  $Fe(OH)_2$  exists when  $pH > 7.8$  and  $FeCO_3$  can only be observed in a narrow range of 6.5–9.2. By referring to the equilibrium pH shown in Table 1 after precipitation of sulfide, all three precipitates might exist in the sediment, while 99.9% sulfide can be removed.

A black sediment was obtained after filtering the solution from the sulfide precipitation process, while after drying at 80 °C in an oven, the black sediment turned dark red (Figure 5a). This might suggest that certain chemical reactions occurred during the drying process. Figure 5b shows the XRD pattern of the dried precipitate; three components were observed, i.e., magnetite ( $Fe_3O_4$ ), troilite ( $FeS$ ), and siderite ( $FeCO_3$ ). Magnetite in the sediment might result from the partial oxidation of  $Fe(OH)_2$  to

$\text{Fe}_3\text{O}_4$ , as shown in Equation (2), with the reaction being spontaneous. According to the results shown in Table 1, 99.9% of sulfide was removed at pH 9.08.

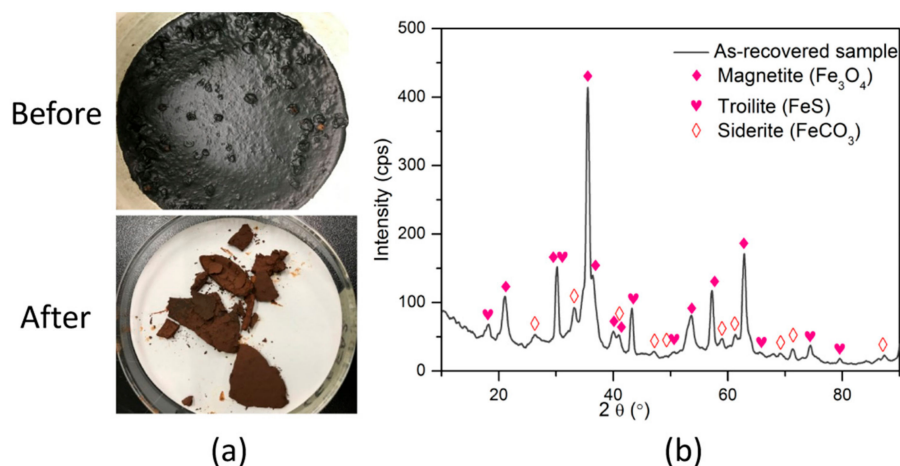


**Figure 5.** XRD pattern of the sediment obtained after the sulfide precipitation process. (a) Photo of the sediment obtained before and after drying (b) XRD pattern of the sediment obtained after drying.

**Table 1.** pH, ion concentrations, and removal ratio in the effluent at different steps of processing.

Parameters	Initial <sup>a</sup>	SRB Treatment <sup>a</sup>	Precipitation <sup>a</sup>	Removal Ratios (%)	WHO Value <sup>a</sup>
pH	7.01	8.86	9.08	NA <sup>b</sup>	6.0–9.0
Pb <sup>2+</sup>	0.924	ODL <sup>c</sup>	ODL	>94.6	0.2
Cd <sup>2+</sup>	2.10	ODL	ODL	>99.8	0.01
SO <sub>4</sub> <sup>2−</sup>	3013.5	27.1	25.2	99.2	300
Ca <sup>2+</sup>	400.1	3.78	3.43	99.1	200
HS <sup>−</sup>	NA	1001	1.27	99.9	1.0
HCO <sub>3</sub> <sup>−</sup>	NA	1278	786	NA	NA
Fe <sup>2+</sup>	NA	NA	89.5	NA	NA

<sup>a</sup> All concentrations were in the unit of mg/L, <sup>b</sup> NA: Not applicable, <sup>c</sup> ODL: out of the detection limit.

#### 4. Conclusions

With the assistance of SRB, 99% of sulfate was first reduced to sulfide and heavy metals while 99% of calcium ions were removed simultaneously after 12 days of reduction with SRB. In the sulfate reduction process, the reaction mechanism for the heavy metal and calcium ion removal was simulated by thermodynamic calculations, which predicted the appearance of  $\text{CaCO}_3$ ,  $\text{PbS}$ , and  $\text{CdS}$ . In the following sulfide precipitation process,  $\text{Fe}(\text{OH})_2$  was selected and tested due to the following facts: 1)  $\text{Fe}(\text{OH})_2$  has poor solubility in aqueous solution which will not introduce new impurity in the effluent; 2) the product resulting from reaction of  $\text{Fe}(\text{OH})_2$  and sulfide, i.e.,  $\text{FeS}$ , is insoluble in aqueous solution, which would help remove excessive sulfide ions thoroughly. The reaction mechanism for sulfide precipitation was also simulated and interpreted with thermodynamic calculations. The predicted results are different from the XRD analysis results due to the oxidation of  $\text{Fe}(\text{OH})_2$  to  $\text{Fe}_3\text{O}_4$ . After the two-step removal process, the overall removal ratio of  $\text{Ca}^{2+}$ ,  $\text{SO}_4^{2−}$ ,  $\text{Pb}^{2+}$ , and  $\text{Cd}^{2+}$  were 99.1%, 99.2%, > 94.6%, and > 99.8%, respectively. The concentration of sulfate, lead, cadmium, and calcium ions in the effluent were significantly lower than the concentration recommended by WHO for wastewater discharge into streams [47], which is considered safe for directly discharged.



**Supplementary Materials:** The following are available online at <http://www.mdpi.com/2071-1050/12/3/1263/s1>.

**Author Contributions:** Methodology, B.F. and J.W.A.; software, S.G.; validation, B.F.; formal analysis, S.G., B.F. and J.W.A.; investigation, B.F.; resources, S.G.; data curation, J.W.A.; writing—original draft preparation, B.F.; writing—review and editing, S.G.; visualization, S.G. and J.W.A.; supervision, B.F.; project administration, J.W.A.; funding acquisition, J.W.A. All authors have read and agreed to the published version of the manuscript.

**Funding:** This research was supported by the National Strategic Project-Carbon Mineralization Flagship Center of the National Research Foundation of Korea (NRF) funded by the Ministry of Science and ICT (MSIT), the Ministry of Environment (ME) and the Ministry of Trade, Industry and Energy (MOTIE). (2017M3D8A2084752).

**Conflicts of Interest:** The authors declare no conflicts of interest. The funders had no role in the design of the study; in the collection, analyses, or interpretation of data; in the writing of the manuscript, or in the decision to publish the results.

## References

1. Dufo-Lopez, R.; Lujano-Rojas, J.M.; Bernal-Agustin, J.L. Comparison of different lead–acid battery lifetime prediction models for use in simulation of stand-alone photovoltaic systems. *Appl. Energ.* **2014**, *115*, 242–253. [\[CrossRef\]](#)
2. Joerissen, L.; Garche, J.; Fabjan, C.; Tomazic, G. Possible use of vanadium redox-flow batteries for energy storage in small grids and stand-alone photovoltaic systems. *J. Power Sour.* **2004**, *127*, 98–104. [\[CrossRef\]](#)
3. Hua, S.; Zhou, Q.; Kong, D.; Ma, J. Application of valve-regulated lead-acid batteries for storage of solar electricity in stand-alone photovoltaic systems in the northwest areas of China. *J. Power Sour.* **2006**, *158*, 1178–1185. [\[CrossRef\]](#)
4. Bhangu, B.S.; Bentley, P.; Sone, D.A.; Bingham, C.M. Nonlinear observers for predicting state-of-charge and state-of-health of lead-acid batteries for hybrid-electric vehicles. *IEEE Trans. Veh. Technol.* **2005**, *54*, 783–794. [\[CrossRef\]](#)
5. Pesaran, A.A. Battery thermal models for hybrid vehicle simulations. *J. Power Sour.* **2002**, *110*, 377–382. [\[CrossRef\]](#)
6. Rydh, C.J. Environmental assessment of vanadium redox and lead-acid batteries for stationary energy storage. *J. Power Sour.* **1999**, *80*, 21–29. [\[CrossRef\]](#)
7. Parker, C.D. Lead-acid battery energy-storage systems for electricity supply networks. *J. Power Sour.* **2001**, *100*, 18–28. [\[CrossRef\]](#)
8. Yin, Y.; Liu, C.; Fan, S. Hybrid energy storage devices combining carbon-nanotube/polyaniline supercapacitor with lead-acid battery assembled through a “directly-inserted” method. *RSC Adv.* **2014**, *4*, 26378–26382. [\[CrossRef\]](#)
9. Sun, Z.; Cao, H.; Zhang, X.; Lin, X.; Zheng, W.; Cao, G.; Sun, Y.; Zhang, Y. Spent lead-acid battery recycling in China-A review and sustainable analyses on mass flow of lead. *Waste Manag.* **2017**, *64*, 190–201. [\[CrossRef\]](#)
10. Zabaniotou, A.; Kouskoumvekaki, E.; Sanopoulos, D. Recycling of spent lead/acid batteries: the case of Greece. *Resour. Conserv. Recy.* **1999**, *25*, 301–317. [\[CrossRef\]](#)
11. Ma, Y.; Qiu, K. Recovery of lead from lead paste in spent lead acid battery by hydrometallurgical desulfurization and vacuum thermal reduction. *Waste Manag.* **2015**, *40*, 151–156. [\[CrossRef\]](#) [\[PubMed\]](#)
12. Jolly, R.; Rhin, C. The recycling of lead-acid batteries: production of lead and polypropylene. *Resour. Conserv. Recy.* **1994**, *10*, 137–143. [\[CrossRef\]](#)
13. Sonmez, M.S.; Kumar, R.V. Leaching of waste battery paste components. Part 2: Leaching and desulphurization of PbSO<sub>4</sub> by citric acid and sodium citrate solution. *Hydrometallurgy* **2009**, *95*, 82–86. [\[CrossRef\]](#)
14. Zhu, X.; Yang, J.; Gao, L.; Liu, J.; Yang, D.; Sun, X.; Zhang, W.; Wang, Q.; Li, L.; He, D.; et al. Preparation of lead carbonate from spent lead paste via chemical conversion. *Hydrometallurgy* **2013**, *134–135*, 47–53. [\[CrossRef\]](#)
15. Gu, S.; Fu, b.; Fujita, T.; Ahn, J.W. Thermodynamic simulations for determining the recycling path of a spent lead-acid battery electrolyte sample with Ca(OH)<sub>2</sub>. *Appl. Sci.* **2019**, *9*, 2262. [\[CrossRef\]](#)
16. Vu, H.H.T.; Gu, S.; Thriveni, T.; Khan, M.D.; Tuan, L.Q.; Ahn, J.W. Sustainable treatment for sulfate and lead removal from battery wastewater. *Sustainability* **2019**, *11*, 3497. [\[CrossRef\]](#)
17. Ma, C.; Shu, Y.; Chen, H. Recycling lead from spent lead pastes using oxalate and sodium oxalate and preparation of novel lead oxide for lead-acid batteries. *RSC Adv.* **2015**, *5*, 94895–94902. [\[CrossRef\]](#)

18. Buldini, P.L.; Saxena, P.; Saxena, V.; Toponi, A. Voltammetric determination of trace amounts of copper, cadmium and lead in lead-acid battery electrolyte. *Analyst* **1990**, *115*, 1073–1075. [\[CrossRef\]](#)
19. Obeng-Gyasi, E. Sources of lead exposure in various countries. *Rev. Environ. Health* **2019**, *34*, 25–34. [\[CrossRef\]](#)
20. Gulson, B.L.; Jameson, C.W.; Mahaffey, K.R.; Mizon, K.J.; Korsch, M.J.; Vimpani, G. Regnancy increases mobilization of lead from maternal skeleton. *J. Lab. Clin. Med.* **1997**, *130*, 51–62. [\[CrossRef\]](#)
21. Hu, H.; Téllez-Rojo, M.M.; Bellinger, D.; Smith, D.; Ettinger, A.S.; Lamadrid-Figueroa, H.; Schwartz, J.; Schnaas, L.; Mercado-García, A.; Hernández-Avila, M. Fetal lead exposure at each stage of pregnancy as a predictor of infant mental development. *Environ. Health Persp.* **2006**, *114*, 1730–1735. [\[CrossRef\]](#)
22. Reuben, A.; Caspi, A.; Belsky, D.W.; Broadbent, J.; Harrington, H.; Sugden, K.; Houts, R.M.; Ramrakha, S.; Poulton, R.; Moffitt, T.E. Association of childhood blood lead levels with cognitive function and socioeconomic status at age 38 years and with IQ change and socioeconomic mobility between childhood and adulthood. *JAMA* **2017**, *317*, 1244–1251. [\[CrossRef\]](#) [\[PubMed\]](#)
23. Obeng-Gyasi, E. Lead Exposure and Cardiovascular Disease among Young and Middle-Aged Adults. *Med. Sci.* **2019**, *7*, 103. [\[CrossRef\]](#) [\[PubMed\]](#)
24. Harari, F.; Sallsten, G.; Christensson, A.; Petkovic, M.; Hedblad, B.; Forsgard, N.; Melander, O.; Nisson, P.M.; Borne, Y.; Engstrom, G.; et al. Blood lead levels and decreased kidney function in a population-based cohort. *Am. J. Kidney Dis.* **2018**, *72*, 381–389. [\[CrossRef\]](#)
25. Lin, J.L.; Lin-Tan, D.T.; Hsu, K.H.; Yu, C.C. Environmental lead exposure and progression of chronic renal diseases in patients without diabetes. *New Engl. J. Med.* **2003**, *348*, 277–286. [\[CrossRef\]](#)
26. Obeng-Gyasi, E.; Armijos, R.X.; Weigel, M.M.; Filippelli, G.; Sayegh, M.A. Hepatobiliary-related outcomes in US adults exposed to lead. *Environments* **2018**, *5*, 46. [\[CrossRef\]](#)
27. Can, S.; Bağci, C.; Ozaslan, M.; Bozkurt, A.I.; Cengiz, B.; Cakmak, E.A.; Kocabas, R.; Karadag, E.; Tarakçioğlu, M. Occupational lead exposure effect on liver functions and biochemical parameters. *Acta Physiol. Hung.* **2008**, *95*, 395–403. [\[CrossRef\]](#)
28. Benatti, C.T.; Tavares, C.R.G.; Lenzi, E. Sulfate removal from waste chemicals by precipitation. *J. Environ. Manag.* **2009**, *90*, 504–511. [\[CrossRef\]](#)
29. Tait, S.; Clarke, W.P.; Keller, J.; Batstone, D.J. Removal of sulfate from high-strength wastewater by crystallization. *Water Res.* **2009**, *43*, 762–772. [\[CrossRef\]](#)
30. Haghsheno, R.; Mohebbi, A.; Hashemipour, H.; Sarrafi, A. Study of kinetic and fixed bed operation of removal of sulfate anions from an industrial wastewater by an anion exchange resin. *J. Hazard. Mater.* **2009**, *166*, 961–966. [\[CrossRef\]](#)
31. Liang, F.; Xiao, Y.; Zhao, F. Effect of pH on sulfate removal from wastewater using a bioelectrochemical system. *Chem. Eng. J.* **2013**, *218*, 147–153. [\[CrossRef\]](#)
32. Jong, T.; Parry, D.L. Removal of sulfate and heavy metals by sulfate reducing bacteria in short-term bench scale upflow anaerobic packed bed reactor runs. *Water Res.* **2003**, *37*, 3379–3389. [\[CrossRef\]](#)
33. Mizuno, O.; Li, Y.Y.; Noike, T. The behavior of sulfate-reducing bacteria in acidogenic phase of anaerobic digestion. *Water Res.* **1998**, *32*, 1626–1634. [\[CrossRef\]](#)
34. Zhao, F.; Rahunen, N.; Varcoe, J.R.; Chandra, A.; Avignone-Rossa, C.; Thumser, A.E.; Slade, R.C.T. Activated carbon cloth as anode for sulfate removal in a microbial fuel cell. *Environ. Sci. Technol.* **2008**, *42*, 4971–4976. [\[CrossRef\]](#)
35. Glombitza, F. Treatment of acid lignite mine flooding water by means of microbial sulfate reduction. *Waste Manag.* **2001**, *21*, 197–203. [\[CrossRef\]](#)
36. Tsibouklis, J.; Stone, M.; Thorpe, A.A.; Graham, P.; Peters, V.; Heerlien, R.; Smith, J.R.; Green, K.L.; Nevell, T.G. Preventing bacterial adhesion onto surfaces: the low-surface-energy approach. *Biomaterials* **1999**, *20*, 1229–1235. [\[CrossRef\]](#)
37. Johnson, D.B.; Hallberg, K.B. Acid mine drainage remediation options: a review. *Sci. Total Environ.* **2005**, *338*, 3–14. [\[CrossRef\]](#)
38. Montgomery, A.D.; McInerney, M.J.; Sublette, K.L. Microbial control of the production of hydrogen sulfide by sulfate-reducing bacteria. *Biotechnol. Bioeng.* **1990**, *35*, 533–539. [\[CrossRef\]](#)
39. Hao, O.J.; Chen, J.M.; Huang, L.; Buglass, R.L. Sulfate-reducing bacteria. *Crit. Rev. Env. Sci. Tec.* **1996**, *26*, 155–187. [\[CrossRef\]](#)

40. Tsukamoto, T.K.; Miller, G.C. Methanol as a carbon source for microbiological treatment of acid mine drainage. *Water Res.* **1999**, *33*, 1365–1370. [[CrossRef](#)]
41. Silva, A.J.; Hirasawa, J.S.; Varesche, M.B.; Foresti, E.; Zaiat, M. Evaluation of support materials for the immobilization of sulfate-reducing bacteria and methanogenic archaea. *Anaerobe* **2006**, *12*, 93–98. [[CrossRef](#)] [[PubMed](#)]
42. Roy, A.; Das, B.K.; Bhattacharya, J. Development and validation of a spectrophotometric method to measure sulfate concentrations in mine water without interference. *Mine Water Environ.* **2011**, *30*, 169–174. [[CrossRef](#)]
43. Clescerl, L.S. *Standard Methods for the Examination of Water and Wastewater*, 20th ed.; American Public Health Association: Washington, DC, USA, 2005; pp. 4310–4500.
44. Wu, J.; Zheng, H. Quantitative measurement of the concentration of sodium carbonate in the system of  $\text{Na}_2\text{CO}_3\text{-H}_2\text{O}$  by raman spectroscopy. *Chem. Geol.* **2010**, *273*, 267–271. [[CrossRef](#)]
45. Ponou, J.; Wang, L.P.; Dodbiba, G.; Matuo, S.; Fujita, T. Effect of carbonation on banana peels for removal of cadmium ions from aqueous solution. *Environ. Eng. Manag. J.* **2016**, *15*, 851–860. [[CrossRef](#)]
46. Xia, H.; Zhan, L.; Xie, B. Preparing ultrafine PbS powders from the scrap lead-acid battery by sulfurization and inert gas condensation. *J. Power Sour.* **2017**, *341*, 435–442. [[CrossRef](#)]
47. WHO. A Compendium of Standards for Wastewater Reuse in the Eastern Mediterranean Region. 2006. Available online: <https://apps.who.int/iris/bitstream/handle/10665/116515/dsa1184.pdf;sequence=1> (accessed on 29 January 2020).



© 2020 by the authors. Licensee MDPI, Basel, Switzerland. This article is an open access article distributed under the terms and conditions of the Creative Commons Attribution (CC BY) license (<http://creativecommons.org/licenses/by/4.0/>).